Pergamon

Ocean Engng, Vol. 22, No. 8, pp. 765–784, 1995

0029–8018/95 $9.50 + .00

0029–8018(95)00016-X

EXPERIMENTAL AND NUMERICAL INVESTIGATIONS OF TETHERED SPAR AND SPHERE BUOYS IN IRREGULAR WAVES

E. B. Carpenter,* J. W. Leonard†‡ and S. C. S. Yim*

*Ocean Engineering Program, Oregon State University, Corvallis, OR 97331, U.S.A.
†Civil Engineering Department, University of Connecticut, Storrs, CT 06269, U.S.A.

(*Received* 20 *January* 1995; *accepted* 15 *February* 1995)

Abstract—A series of large-scale experiments were conducted to examine the motions of buoys in a variety of wave climates. In conjunction with these experiments, numerical simulations of selected tests were conducted to test the present ability of a particular computer program to model buoy responses. This paper considers individual wave tests for two of the buoy models used in the experiments, a spar buoy and a sphere buoy. The wave field is generated using a JONSWAP spectrum. A description of the experiments shows that each buoy is subject to significant resonant responses, in heave for the spar and surge for the sphere, even though wave forcing is not present at or immediately adjacent to the resonant frequencies. The numerical simulations show generally good comparisons with the experimental data.

1. INTRODUCTION

The behavior of tethered buoys in random seas is not well understood. However, these buoys find many uses in ocean applications. One of the primary uses for deep ocean buoys is the collection and telemetry of atmospheric and ocean data as part of the National Buoy Data Center program (Steele *et al.*, 1992). Other uses include collection and transmission of acoustic data (Tattersall *et al.*, 1992) and experimental methods for the conversion of wave energy to electricity (Salomon, 1989). There are many uses for tethered deep sea buoys, and to allow for better use of tethered buoy systems, it is necessary to develop an adequate experimental database concerning tethered buoy motions and buoy mooring dynamic behavior.

A series of experiments studying the dynamic behavior of tethered buoys in deep water was conducted in April 1992 at Oregon State University. These experiments supply much needed data regarding the behavior of tethered buoys. Also, they provide data which is useful for the validation of computer algorithms designed to simulate buoy-cable systems. The uniqueness of these experiments is that they attempt to model several general buoy shapes in very deep water.

There has been relatively little work regarding tethered buoy behavior published in the engineering literature. Some researchers have studied the behavior of freely floating buoys and there has been much work published pertaining to the response of cables to hydrodynamic loadings.

‡ Author to whom correspondence should be addressed.

Halliwell and Harris (1988) studied the low frequency motions of ships tethered with a single-point mooring. Witz *et al.* (1989) examined the roll response of semi-submersibles. Ostergaard and Schellin (1987) compared the experimental and theoretical behavior of floating offshore structures. However, their emphasis was on ship forms and semi-submersibles also. Jenkins *et al.* (1993) present the results of regular wave tests for a spar buoy based on the same experiments detailed in this paper.

Sundaravadivelu *et al.* (1991) conducted an experimental study of the behavior of a buoy with a single point mooring system. They found that for constant wave steepness, the surge and heave accelerations and dynamic cable tension increase as the relative water depth (d/L) decreases. However, the scope of their study considered only the behavior of a sphere buoy under the influence of regular waves.

Dorman (1972) examined a prototype study of an unmoored spar buoy and found that the spar buoy was a surface follower for low-frequency waves but that it filtered out the higher frequency waves. This means that the observed amplitudes of the buoy response were proportional to the incident wave amplitudes for long period waves but that short waves caused minimal response.

The primary objective of this research is to examine experimental data regarding the behavior of tethered buoy systems. The behavior of interest includes the buoy motion in six degrees of freedom and the mooring line tension.

The second objective of this work is to consider the results of an attempt to model the measured buoy system responses using the KBLDYN computer program (Chiou, 1989). The purpose of this comparison is to determine the capability of the existing algorithm to model realistic situations successfully. Such a comparison may provide guidelines for the development of the next generation of design tools.

This paper examines the previously mentioned experiments modelling the moored buoy responses to various loading conditions at a scale of 1:6. The systems consist of a single-point buoy mooring. The buoy models include spar (cylinder), sphere, and discus buoys. Results for the spar and sphere buoys are presented in this paper, whilst a discussion of the discus buoy appears in Carpenter *et al.* (1994). Carpenter (1993) provides a detailed discussion for all buoys. The scaled buoy models are in deep ($d/L > 1/2$) to intermediate ($1.2 > d/L > 0.05$, where d = wave length) water, which is analogous to expected prototype environmental conditions. This paper presents results from selected irregular wave tests for the spar and sphere buoy shapes used in the experiments. The results are presented in the form of spectral responses. Additionally, this paper presents the results of numerical simulations of the same test cases.

Section 2 contains a description of the experimental apparatus and procedures used in this study. Section 3 presents the results of representative experimental test cases. Section 4 gives the results of the numerical simulations and compares them with the experimental results. Section 5 contains a summary and conclusions with recommendations for future research.

2. DESCRIPTION OF EXPERIMENT

The experimental program was conducted at the Oregon State University O.H. Hinsdale Wave Research Laboratory in April 1992. All tests were conducted in the large two-dimensional wave channel, which is 342 feet long, 12 feet wide, and 15 feet deep in the experimentation section. A sketch of the wave channel, including special

equipment used for this experiment, appears in Fig. 1. Waves are generated by a large, hydraulic-driven flap-type wave maker.

To provide a deep water mooring while also providing a sufficiently energetic wave climate, the average still water depth in the test section of the channel was 11.3 feet, leaving 3.7 feet of freeboard for waves. Scaling procedures and calibration techniques for these experiments are described in Jenkins *et al.* (1995).

This paper examines two of three different buoy shapes. The buoys used were a spar (cylinder) buoy, a sphere buoy, and a discus buoy which is discussed in greater detail in Carpenter *et al.* (1994). These buoys were selected to span the range of buoy types commonly used.

The spar buoy represents one extreme in the range of buoy shapes since its motions are not necessarily coupled with the water surface profile. The discus buoy represents a commonly used shape intermediate to the other two buoys in behavior. Sketches of the three buoys appear as Figs 2 and 3, respectively. Table 1 includes the weights, moored and unmoored drafts, the location of the center of gravity relative to the bottom surface of the buoy (KG), the metacentric height (GM), moments of inertia, added mass coefficients, damping ratios and heave, surge, and pitch natural frequencies for each of the buoys used in these experiments.

The spar buoy is a cylinder 6.35 inches in diameter and 50 inches long. It is made

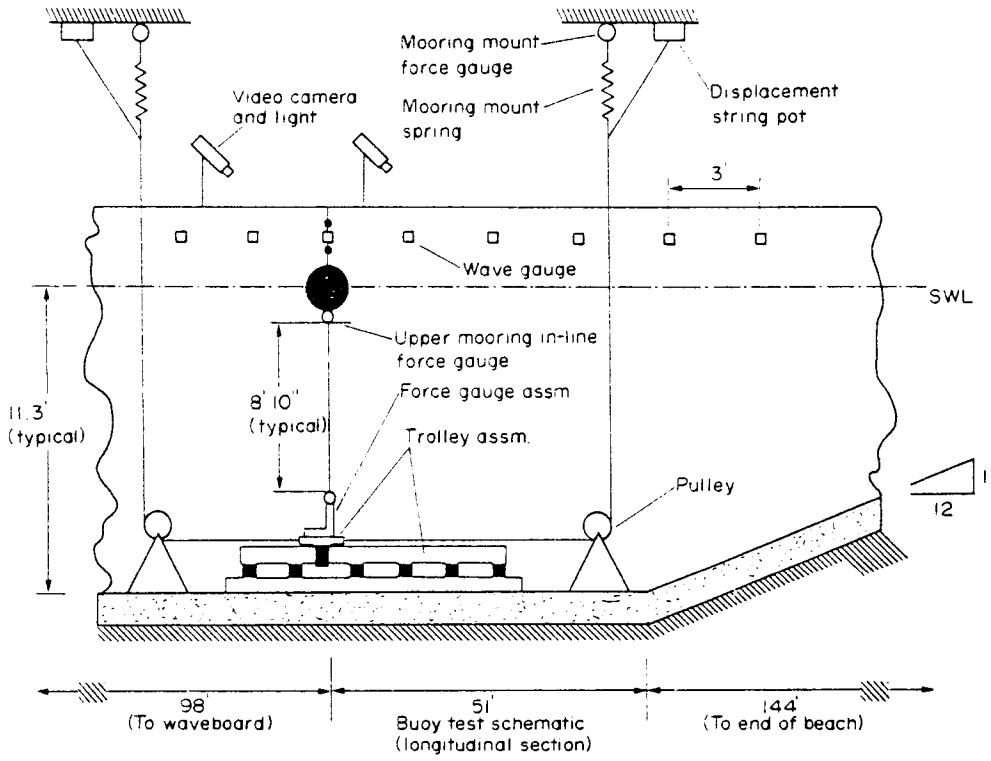

Fig. 1. Wave channel configuration for buoy tests.

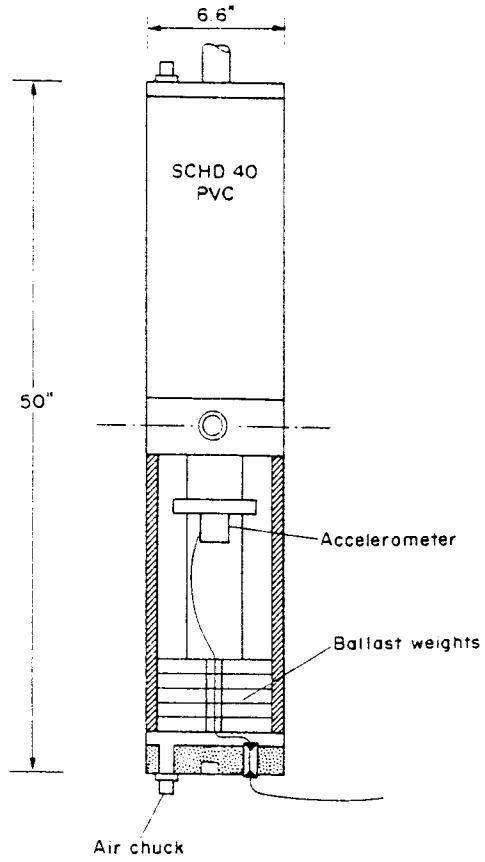

Fig. 2. Spar buoy.

of two hollow plastic sections connected to a solid plastic center section and end caps. The hollow sections may be used to carry instrumentation and/or ballast. The solid center section provides a guide path for the impulse response tests. The top end cap is designed to receive a tracking rod for the video measurements, while the bottom end cap is used for the tether connection.

The sphere buoy is 13.5 inches in diameter. It was produced by casting foam around a 4.5 inch diameter version of the spar buoy. A hard outer shell is provided as protection for the soft foam. By using the smaller version of the spar buoy in this model, it has the same ability to accept instrumentation and ballast in the core of the buoy as well as receiving the tracking rod and tether connection.

To assure an initial vertical orientation, all buoys were able to be balanced by external weight application. This was necessary to provide a common initial condition for the video measurements.

The selected mooring cable was 5/16 inches outside diameter (OD) surgical rubber tubing. The tension–strain curve for this material is shown in Fig. 4.

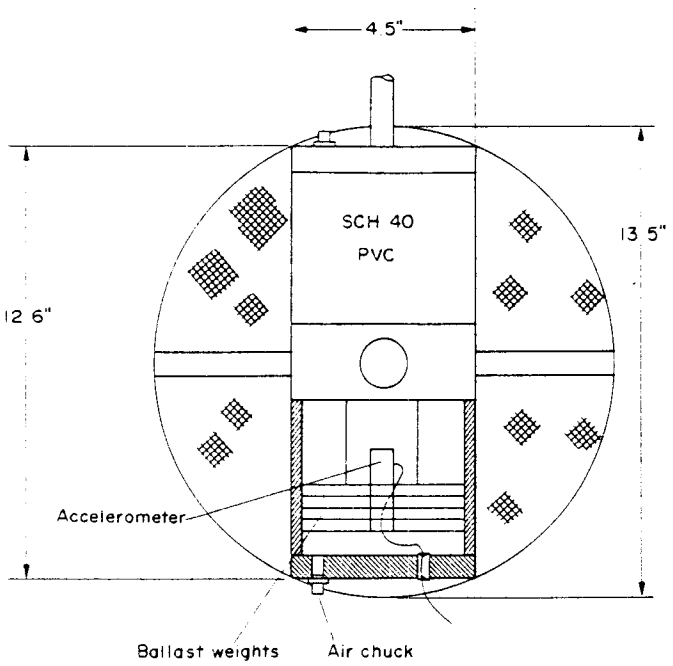

Fig. 3. Sphere buoy.

Table 1. Buoys' intrinsic properties

Property/buoy	Spar	Sphere
Dry weight (lb)	45.3	17.1
Unmoored draft (ft)	3.06	0.444
Moored draft (ft)	3.38	0.485
KG (ft)	1.15	0.440
I_2, I_3 (slug-ft^2)	2.64	0.178
GM (ft)	0.11	0.055
Heave added mass c_a	0.0782	0.624
Added mass moment of inertia c_f	18.7	0.091
Heave damping ratio ζ_1	0.01986	0.10557
Surge/sway damping ratio ζ_2	—	0.16611
Heave natural frequency (Hz)	0.524	1.41
Surge natural frequency (Hz)	0.064	0.115
Pitch natural frequency (Hz)	0.394	0.719

Instrumentation used in this experiment included video measurement equipment, a unidirectional accelerometer, force transducers, and resistance-type wave gauges. Buoy motions in global coordinates were measured using advanced video techniques (Jenkins *et al.*, 1995). Buoy accelerations in local coordinates were measured using an accelerometer. Cable tensions were measured using various strain-gauge-based force transducers. Water surface profiles were obtained using resistance-type wave gauges.

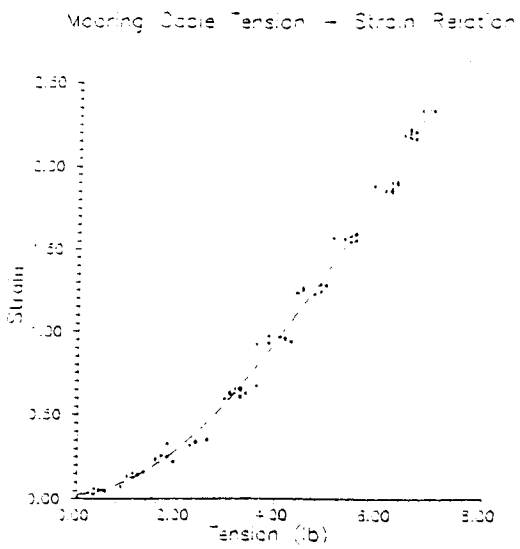

Fig. 4. Tension–strain relationship for mooring cable.

Motion data were measured using advanced video imaging technology. The displacements of two reflective targets rigidly mounted on the buoy were recorded. From this data, the translational and rotational displacements, velocities and accelerations could be calculated. Six high-quality video cameras were used to collect the data. The locations of these cameras are shown in Fig. 1. For a detailed description of the motion measurement techniques see Jenkins *et al.* (1995).

As a redundant buoy motion measuring system, a single-axis accelerometer was mounted inside the buoys for all tests. For the wave tests, the accelerometer was aligned to measure accelerations in the local heave direction. For the impulse-response tests, the accelerometer was aligned to measure translational accelerations for the degree of freedom under consideration, when appropriate.

Force transducers measured cable tensions at the buoy-tether connection point and at the tether bottom connection. At the buoy-tether connection and the bottom connection, linear force rings were utilized. At the bottom connection, a three-dimensional force gauge measured the three orthogonal components of cable tension. The design of the three-dimensional force gauge was first proposed by Leonard (1989). The gauge used in the experiments was based on that design.

All force transducers were pre- and post-calibrated for these tests. The three-dimensional force gauge was calibrated by loading and unloading it with known weights several times. The gauge was loaded in each of the three measurement directions. This was necessary to determine the cross-loading effects. There was no significant hysteresis noted for any of the force transducers.

Water surface profile measurements were made using resistance-type wave gauges. These are industry standard devices which output a varying voltage signal which is linearly related to the water surface elevation variation. The locations of these gauges are shown in Fig. 1. The wave gauges were calibrated using a standard linear displace-

ment method. This gives a linear relationship for change in water surface height to change in measured voltage. Realizations of JONSWAP spectra were input to the wave board. Figure 5 displays sample wave spectra obtained from measurements at the wave gauges for two realizations.

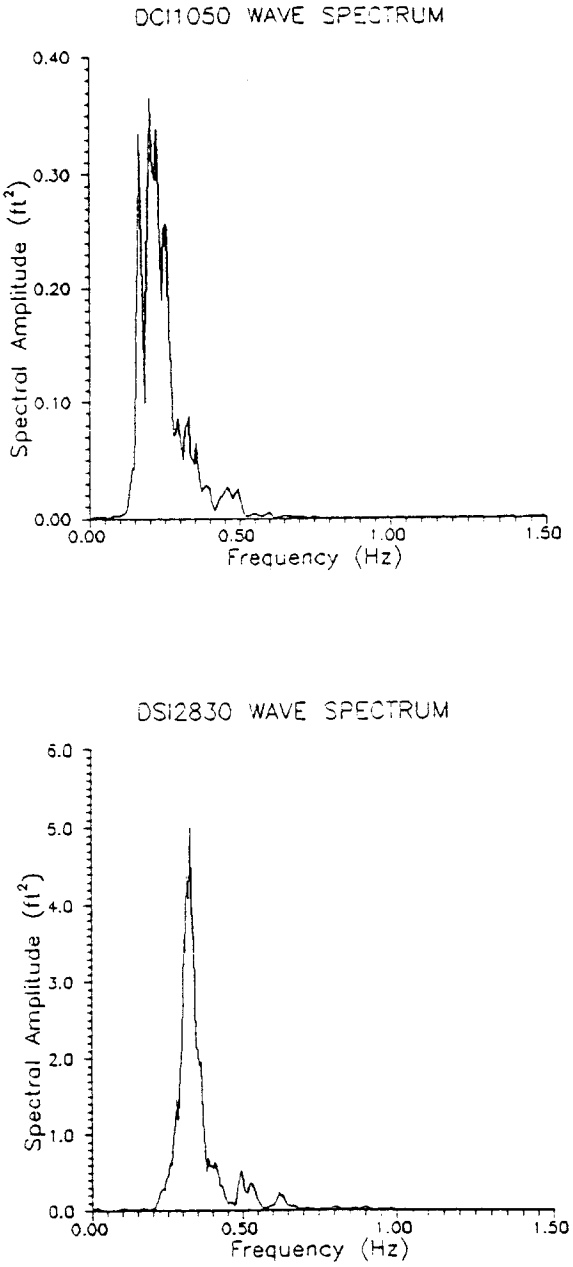

Fig. 5. Wave spectra for spar and sphere buoy tests.

3. EXPERIMENTAL RESULTS

This section describes the results obtained from selected experimental tests. Because these are random wave tests, the results are presented spectrally, to show the frequency dependency of the buoy responses.

3.1. *Spar buoy system response*

Test case DCI1050 (Dynamic response, Cylinder buoy, Irregular wave realization of a JONSWAP spectrum with significant wave height 1.0 feet, significant wave period 5.0 seconds) is presented here (note the nomenclature used for test identification, this short hand will be used to identify the different test cases).

Figure 6(a) presents the heave displacement autospectrum for this test. The heave response for the spar buoy is dominated by the resonant frequency for this buoy system. The numerical simulation in Fig. 6(b), as well as those in Figs 7(b)–13(b) to follow, will be considered in a subsequent section. The amplitude of the heave displacement in Fig. 6(a) is greater than the incident wave amplitude. This is expected due to the small damping ratio and added mass of the buoy. This spectrum shows that the spar buoy heave displacement exhibits a predominant response at the peak incident frequency. However, the data also show a significant response at approximately 0.53 Hz. This is the heave natural frequency for the moored buoy. The associated resonant response at this frequency is significant, even for this test, where the incident wave energy is relatively insignificant at the resonant frequency. This seems to indicate that the spar buoy used in this test is quite sensitive to even small amounts of energy at its natural frequency.

The surge displacement autospectrum for this test appears in Fig. 7(a). The surge response of this buoy seems to depend primarily on the incident wave spectrum and demonstrates that this response is almost entirely dominated by the peak incident wave frequency. It should be noted that there is a minor spectral peak at about 0.068 Hz. This is the resonant frequency for the buoy in surge. From this, we can infer that the spar buoy is less likely to respond resonantly in surge than in heave since the resonant response is fairly weak.

Figure 8(a) presents the pitch displacement angle autospectrum for the tests. Due to the relatively large restoring moment arm presented by the spar buoy, one can expect to see a measurable pitch response. The pitch displacement spectra indicate that the response energy is bimodal with appreciable peaks at approximately 0.025 Hz and 0.7 Hz. Neither of these frequencies relates to a resonant response. The lack of stronger responses at the incident frequencies for these tests is interesting but not necessarily alarming since pitch response depends largely on wave steepness rather than height.

The autospectrum for the cable tension response at the buoy-tether connection point appears in Fig. 9(a). One can expect the cable tension response to bear similarities to the displacement responses since the displacements are largely responsible for the mooring forces. In this case one would expect to see appreciable response at the peak incident wave frequency due to the heave displacement and surge motions and another peak at the heave natural frequency due to the resonant response. The tension measurements indicate that a significant portion of the response is concentrated at the incident wave frequency. As expected, an equally significant response appears at the buoy's heave natural frequency.

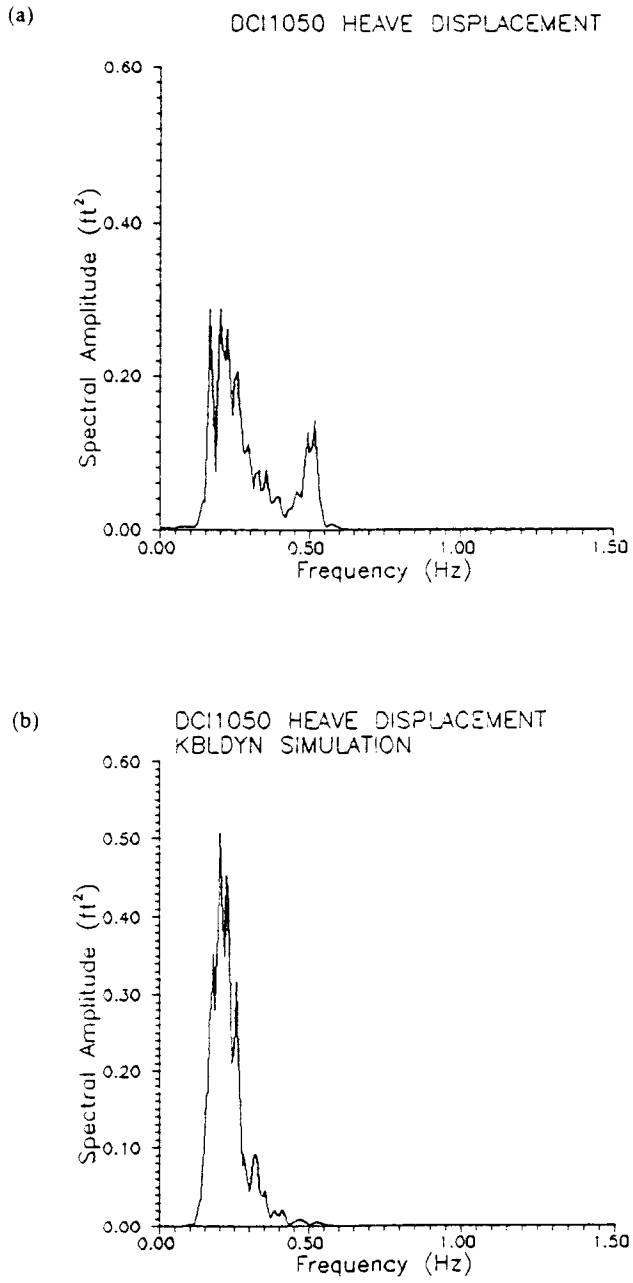

Fig. 6. Spar buoy heave displacement autospectra: (a) experimental measurement, (b) numerical simulation.

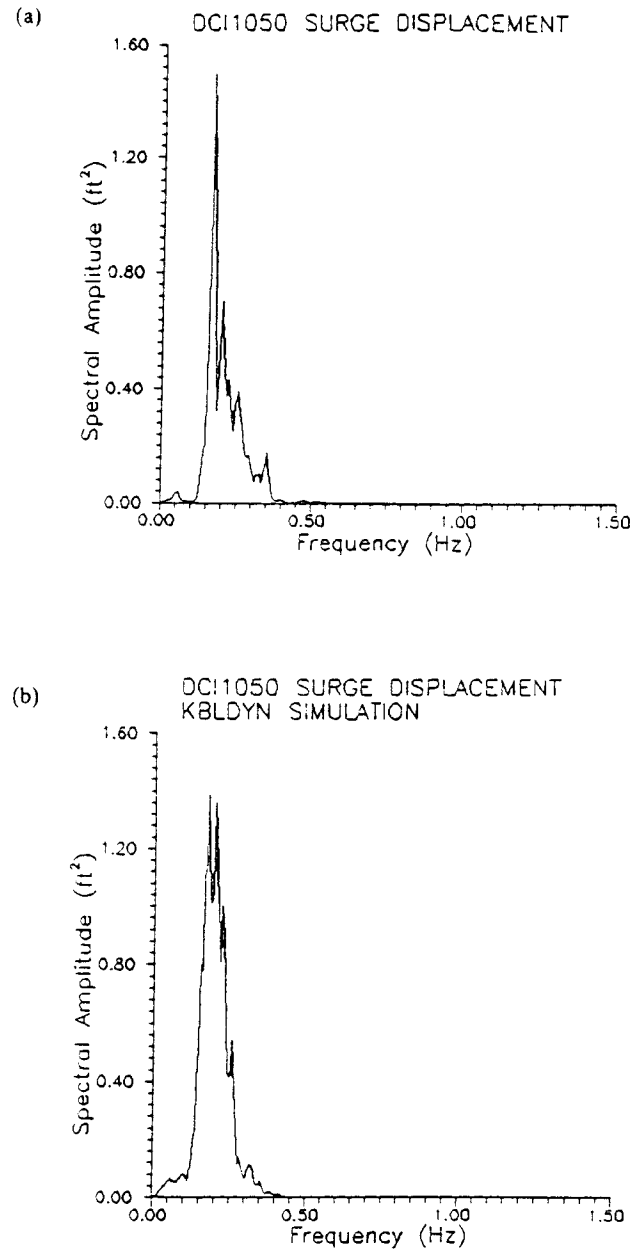

Fig. 7. Spar buoy surge displacement autospectra: (a) experimental measurement, (b) numerical simulation.

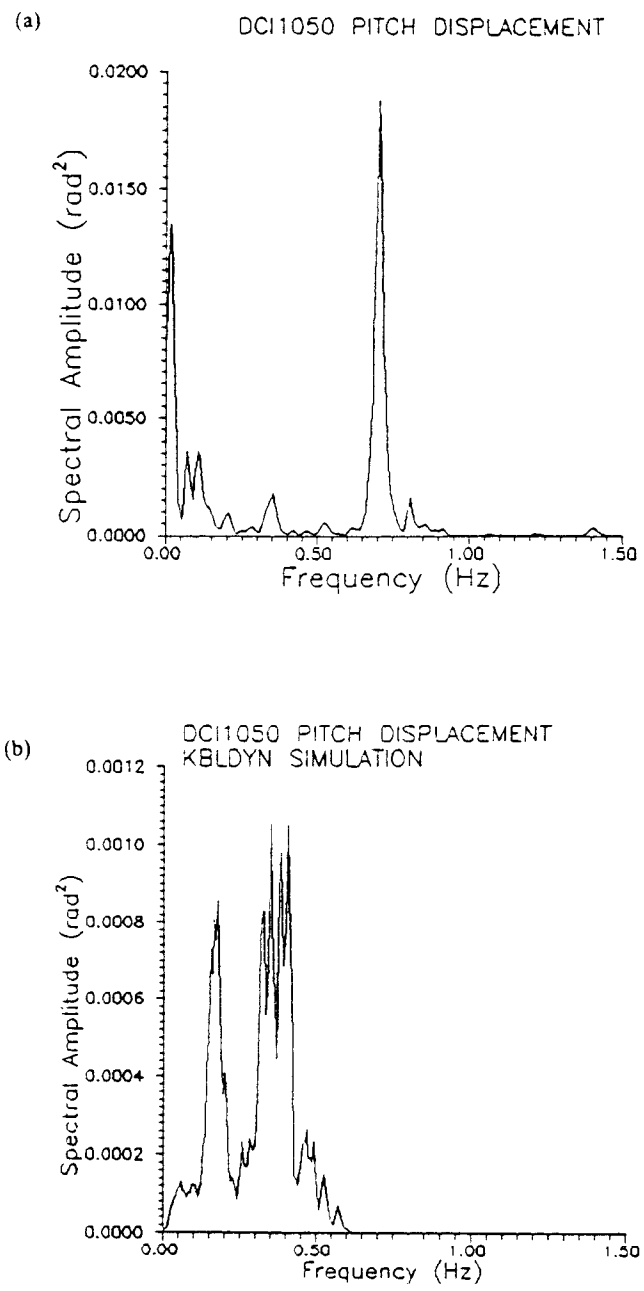

Fig. 8. Spar buoy pitch displacement autospectra: (a) experimental measurement, (b) numerical simulation.

(a)

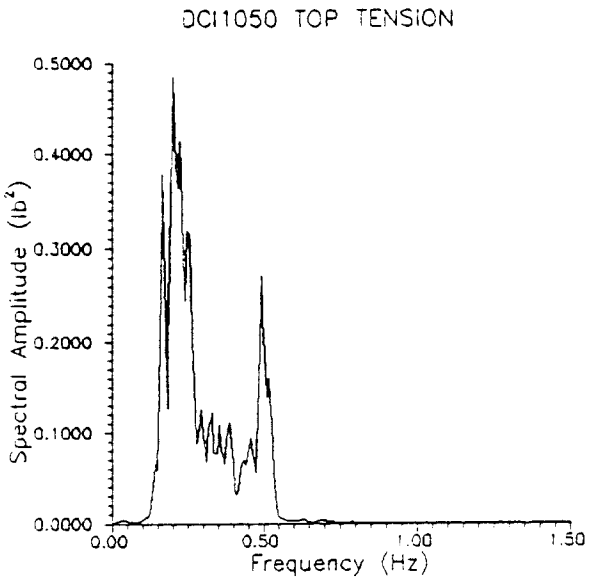

(b)

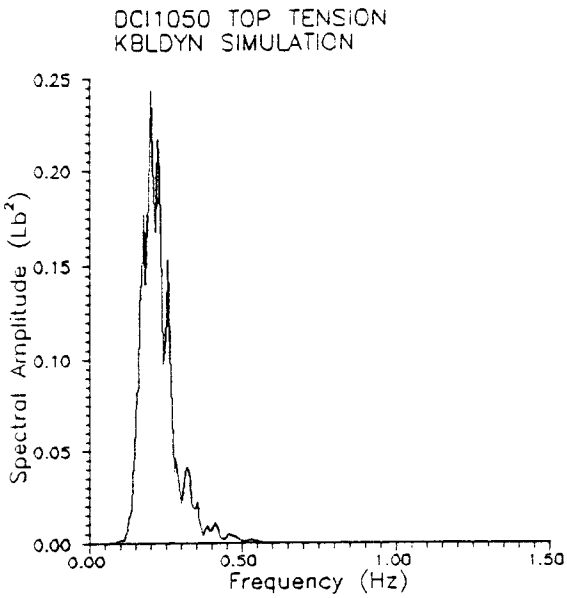

Fig. 9. Spar buoy upper tension autospectra: (a) experimental measurement, (b) numerical simulation.

3.2. *Sphere buoy system response*

For the sphere buoy, test DSI2830 (Dynamic response, Sphere buoy, Irregular wave case, significant wave height 2.8 feet, significant wave period 3.0 seconds) is presented.

Figure 10(a) shows the heave displacement autospectrum for the sphere buoy. This

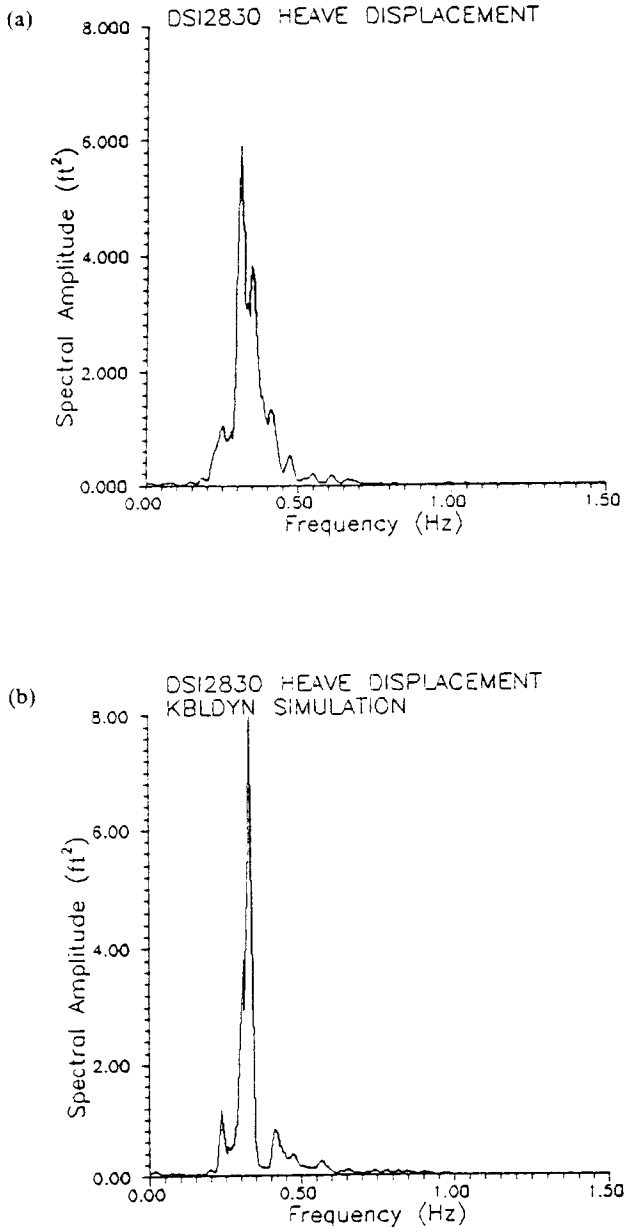

Fig. 10. Sphere buoy heave displacement autospectra: (a) experimental measurements, (b) numerical simulation.

buoy shape is expected to behave similarly to a discus buoy in heave, since it presents a relatively large water plane area, that is, it should be a surface follower.

This displacement spectrum indicates that the peak incident frequency dominates this response. The magnitude of this response is approximately the same as the magnitude of the incident waves. Thus the sphere buoy does appear to be a surface follower in heave.

The heave velocity and acceleration spectra show that the peak incident wave frequency continues to dominate. However the acceleration spectra do indicate some noticeable higher frequency response components. A relatively large peak appears at approximately 1.4 Hz which is the natural frequency for this degree of freedom.

Figure 11(a) shows the surge displacement autospectrum. Relatively small surge motions are expected for the sphere buoy due to its small drag area. In this test, one can see a strong low-frequency response. This response is quite near the resonant frequency for this degree of freedom. This response is significant, since the incident wave spectrum [Fig. 5(b)] shows virtually no forcing at this frequency.

The pitch response appears as a broad-band noise, Fig. 12(a), with significant low-frequency response. The response spectrum for this test does show a fairly strong response. This response is consistent with the expected response for this buoy. Generally, one expects a rather weak pitching response from a sphere buoy because it has a theoretical radiation coefficient of zero, meaning that it does not have a moment arm to cause rotation. The presence of the video tracking rod most probably causes most of the measured pitch response.

Figure 13(a) presents the autospectrum for tether tensions measured at the buoy-cable connection point. Again, the tension response frequencies are expected to be the same as the response frequencies for the translational responses. The tension response spectrum indicates that the peak incident wave frequency dominates the cable response. The spectrum demonstrates a noticeable very low-frequency response for the cable. The low frequencies seen in the tension measurements are not the same as were seen in the surge displacement.

4. NUMERICAL SIMULATIONS

This section discusses the results obtained from the KBLDYN simulations of the selected irregular wave tests. These results are compared to the experimental results to determine the ability of KBLDYN to simulate these experiments.

The KBLDYN algorithm was originally developed by Chiou (1989) and has undergone continuous development since then, including during this study. Comprehensive discussions of the algorithm appear in Chiou (1989) and Chiou and Leonard (1991). In brief, KBLDYN is a mathematical model formulated as a two-point boundary problem which is transformed into an iterative set of quasi-linearized boundary value problems. These quasi-linearized boundary value problems are decomposed into a set of initial value problems. Thus, spatial integration may be performed along the cable. The solutions of the initial value problems are recombined so that the boundary conditions are satisfied.

For this study, the boundary condition at the bottom connection of the cable required that point to be temporally stationary. Thus the velocity at that point was zero at all times. At the tether-buoy connection, the body boundary condition is applied. That

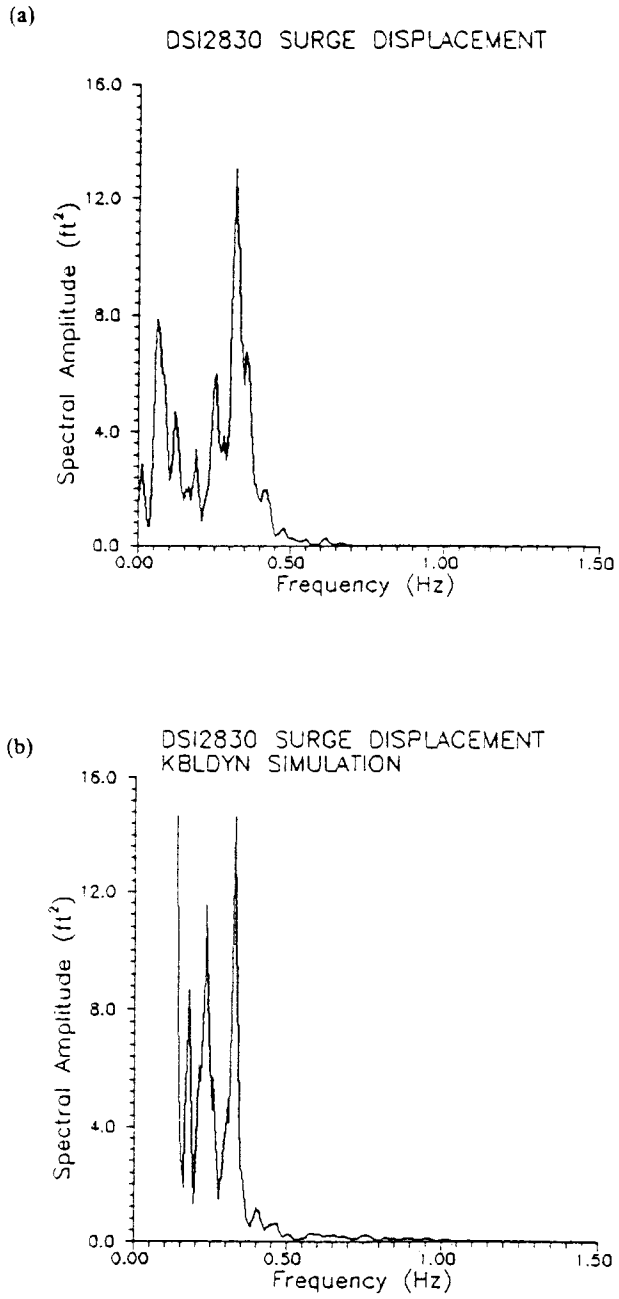

Fig. 11. Sphere buoy surge displacement autospectra: (a) experimental measurements, (b) numerical simulation.

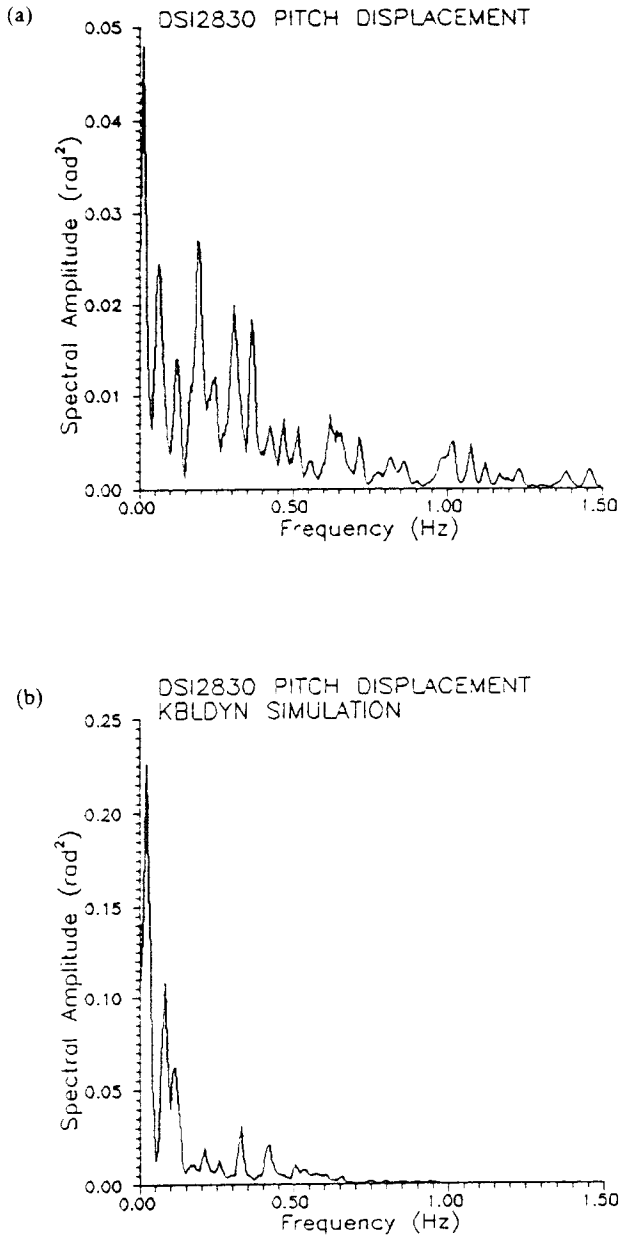

Fig. 12. Sphere buoy pitch displacement autospectra: (a) experimental measurements, (b) numerical simulation.

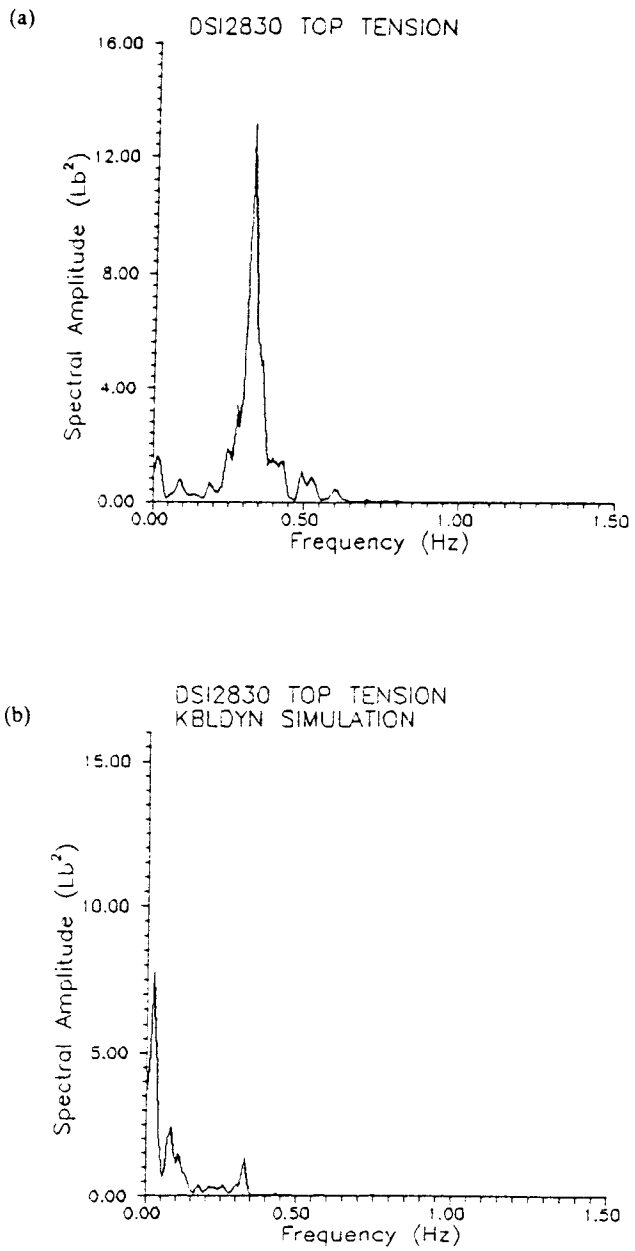

mer , (b) numerical

Fig. 13. Sphere buoy upper tension autospectra: (a) experimental measurements, (b) numerical simulation.

is, the cable must always remain connected to the buoy tether point. This requires that the motion of that point be the same as the motion of the buoy tether point.

Numerical simulations were configured to match the experimental cases as closely as possible. For the irregular wave cases, this required approximating the measured

wave spectrum as a series of 250 or more sine waves. The amplitudes and frequencies for these terms were determined from the measured wave spectrum. The spar and sphere buoys were modelled directly by KBLDYN subroutines.

Since the mooring material is viscoelastic, the initial length of the cable was adjusted for each simulation so that the measured initial cable tension and buoy draft were adequately matched. The initial mooring line tensions were obtained from the force gauge records for each test. The buoy draft is a direct function of the static tension, so the initial buoy draft could also be determined. The mooring cable was modelled as a third order polynomial fit to measured load extension data (Fig. 5). The viscoelastic properties are not currently modelled by KBLDYN but for the short time spans involved, they should not play a significant role in the response.

4.1. *Spar buoy system response*

The heave displacement autospectrum for the KBLDYN simulation appears in Fig. 6(b). The KBLDYN simulation of the heave motions shows the response to be primarily influenced by the peak incident wave frequency. There is, however, a small response evident at the buoy resonant frequency. However, the experimental data show a significant response at the resonant frequency (0.53 Hz), while the simulation shows a less energetic response at this frequency. Also the peak amplitudes of the measured and simulated responses are somewhat different. An additional indicator that KBLDYN may have underpredicted this response is the differences in the variances (as a measure of the total response energy) of the measured and simulated displacements. The measured heave displacement variance is 52.764 in.^{2}, while the simulated variance is only 39.034 in.^{2}. This is most likely due to the relatively weak resonant response in the simulation.

The surge displacement autospectrum for the KBLDYN simulation appears in Fig. 7(b). The KBLDYN simulation of the surge motion shows the response concentrated around the incident wave frequency. However, noticeable peaks do occur at low frequency in the displacement spectrum.

Figure 8(a) shows the pitch displacement spectrum from the KBLDYN simulation. The KBLDYN simulation shows a small but well defined response for the pitch motion of the spar buoy. This response shows peaks at the incident peak frequency and at a frequency of approximately 0.4 Hz. This second peak corresponds to the approximate pitch natural frequency of the buoy. In contrast with the experimental measurements for this degree of freedom, the response is much more well defined, and the experimental data do not show a response at the resonant frequency.

Figure 9(b) shows the top tension autospectrum from the KBLDYN simulation. The KBLDYN simulation of the mooring line tension shows the response concentrated at the peak incident frequency, just as the motions were. The simulation does not show appreciable response associated with the heave resonance, although a small response does occur at the frequency.

4.2. *Sphere buoy system response*

Figure 10(b) presents the KBLDYN simulation of the heave displacement autospectrum. The simulation generally compares well with the experimental results for the heave responses. The spectral representations of the simulated responses and measured

responses are quite similar. Figure 11(b) presents the KBLDYN simulation of surge displacement. The simulation of surge displacement indicates that KBLDYN overpredicts the low-frequency surge displacement relative to the experimental data. The simulated response is dominated by an extremely strong low-frequency response which was not found in the experimental data. The response of the simulation of the incident frequency does seem to have the same magnitude as the measured response, but this is overwhelmed by the energetic low frequency response.

Figure 12(a) presents the simulated pitch displacement for this test. The KBLDYN simulation predicts a strong, well defined pitching motion for the sphere buoy. As discussed above, this is not the expected result.

Figure 13(b) shows the simulated top (buoy-tether connection) dynamic tension. The KBLDYN simulation of the cable tension again shows the low-frequency dominance found in the surge displacement. This is to be expected since the strength of the surge low-frequency response would necessitate large tensions at the frequency.

5. SUMMARY AND CONCLUSIONS

A series of experiments examining the behavior of buoys tethered in deep water has been presented. The results of selected tests have appeared in the form of autospectra and statistics. Additionally, numerical simulations of some tests were presented to demonstrate the present ability of the KBLDYN computer program to simulate the behavior of tethered buoys. The results of these simulations were presented in the same format as the experimental data.

5.1. *Conclusions*

1. The spar buoy response in heave is dominated by the resonant frequency. Therefore, this type of buoy should be designed so that the heave natural frequency is far away from any possible input frequencies.
2. The strength of the spar buoy's resonant heave response requires careful attention for buoy–tether design. This is due to the fact that much of the response energy for heave motions and cable tensions seems to concentrate at this frequency.
3. The sphere buoy's surge response may be highly dependent on its natural frequency. This is true for displacement only, since velocities and accelerations occur at higher frequencies.
4. The sphere moored buoy system exhibits predominant responses at the incident wave frequencies. The amplitudes of these responses indicate that this buoy is a surface follower for heave.
5. The numerical simulations of spar and sphere buoys seem to provide acceptably accurate predictions in comparison with the experimental data. The acceptability of the predictions depends on the requirements of the user, however.

5.2. *Recommendations for research*

1. A viscoelastic model should be implemented in the KBLDYN program. This is especially important due to the increasing use of cables with viscoelastic properties.
2. An improved buoy modelling algorithm should be implemented in KBLDYN with large rotation capability. Such an algorithm should include the possibility of modelling the buoys using diffraction theory. This will allow for simulation of the large buoys used in deep water applications.

3. Future experimental studies should be conducted to consider the effects of using other mooring materials, using composite moorings (i.e. several materials), and using multileg moorings.

Acknowledgement—The work described in this paper was conducted under Naval Civil Engineering Laboratory contract N47408-90-C-1146.

REFERENCES

Carpenter, E.B. 1993. An experimental and numerical investigation of tethered buoy motions in irregular waves. M.Sc. thesis (part), Oregon State University.

Carpenter, E.B., Idris, K., Leonard, J.W. and Yim, S.C.S. 1994. Behavior of a moored discus buoy in an Ochi-Hubble wave spectrum. In *Offshore Mechanics and Arctic Engineering Conference Proceedings*, Houston, May 1994.

Chiou, R. 1989. Nonlinear hydrodynamic response of curved singly-connected cables. Ph.D. thesis (part), Oregon State University.

Chiou, R. and Leonard, J.W. 1991. Nonlinear hydrodynamic response of curved singly-connected cables. In *Proc. Computer Modeling in Ocean Engineering*, Barcelona, pp. 412–424.

Dorman, C.E. 1972. Motions of a small spar buoy. M.Sc. thesis (part), Oregon State University.

Halliwell, A.R. and Harris, R.E. 1988. A parametric experimental study of low-frequency motions of single point mooring systems in waves. *Appl. Ocean Res.*, **10**, 74–86.

Jenkins, C.H., Leonard, J.W., Walton, J.S. and Carpenter, E.B. 1995. Experimental investigations of moored buoys using advanced video techniques. *Ocean Engng*, **22**, 317–335.

Jenkins, C.H., Idris, K., Leonard J.W. and Yim, S.C.S. 1993. Dynamic response of a spar buoy: an experimental/numerical comparison. *Offshore Mechanics and Arctic Engng Conf. Proc.*, Glasgow.

Leonard, J.S. 1989. Experimental characterization of mooring system in waves and an introduction to bi-scaling. Ph.D. dissertation, University of California, Santa Barbara.

Ostergaard, C. and Schellin, T.E. 1987. Comparison of experimental and theoretical wave actions on floating and compliant offshore structures. *Appl. Ocean Res.*, **9**, 192–213.

Salomon, R.E. 1989. Rocking buoy wave energy converter. *Ocean Engng*, **16**, 319–324.

Steele, K.E., Teng, C.C. and Wang, D.W.C. 1992. Wave direction measurements using pitch-roll buoys. *Ocean Engng*, **19**, 349–375.

Sundaravadivelu, R., Harikrishna Babu, M. and Murugaganesh, R. 1991. Experimental investigation on a single point mooring system. *Ocean Engng*, **18**, 405–417.

Tattersall, J.M., King, P.C. and Mingrone, J.A. 1992. The acoustic transient recording buoy (ATRB): system description and initial measurement results. *IEEE J. Oceanic Engng*, **18**, 227–238.

Witz, J.A., Ablett, C.B. and Harrison, J.H. 1989. Roll response of semisubmersibles with nonlinear restoring moment characteristics. *Appl. Ocean Res.*, **11**, 153–166.

Pergamon

TIME
DIMENS

*Department of

†Department of Eng

(*Receiv*

Abstract—The tw
using potential flo
step two numeric
the complex plane
the solution is ob
The other approa
shape functions ar
are obtained for
provided for a cir
element method is
element method

Wave loading on l
linearized velocity
ation, such as the v
useful in many ca
resonances at wave
theory means that
varying drift forces
can be captured by
the prediction of w
practice, however,
unworkable. On th
disturbances are re
undesirable and ha

The fully nonline
that the wave profil
The problem can
enables us to find
law will give the n
further gives the n
free surface will gi